Degradation of Ni-YSZ and Ni-GDC fuel cells after 1000 h operation: Analysis of different overpotential contributions according to electrochemical and microstructural characterization

Aiswarya Krishnakumar Padinjarethil[1], *Fiammetta Rita* Bianchi[2,*], *Barbara* Bosio[2], and *Anke* Hagen[1]

[1] Department of Energy Conversion and Storage, Technical University of Denmark, Building 310, Fysikvej, DK-2800 Lyngby, Denmark
[2] DICCA, University of Genoa, Via Opera Pia 15b, 16145 Genoa, Italy

Abstract. Solid Oxide Fuel Cell (SOFC) technologies are emerging as potential power generation units with limited environmental impacts. However, the main challenges towards large scale commercial applications are high costs and low lifetime compared to currently used technologies. The present study aims at understanding degradation mechanisms in SOFCs through both experimental and modelling approaches. For this purpose, two state of the art fuel cell configurations based on Ni cermet fuel electrode (either YSZ-Yttrium Stabilised Zirconia or GDC-Gadolinium Doped Ceria), YSZ electrolyte and LSCF (Lanthanum Strontium Cobalt Ferrite oxide) air electrode were chosen. The cells were tested for 1000 hours with H_2 rich mixture as fuel feed and air as oxidant. Cells were characterised at several H_2/H_2O ratios and temperatures with air or oxygen fed to the air electrode using different techniques. These allowed the identification of kinetic parameters to be implemented in an in-house 2D Fortran based model. The model was able to successfully simulate global cell behaviour as a function of local features, and it was validated with experimental I-V curves recorded prior and post durability operation. Moreover, post-mortem microstructure characterisation was also performed to fine-tune the model towards a more accurate prediction of the degradation influence on cell performance.

1. Introduction

Solid Oxide Fuel Cells (SOFCs) are promising energy conversion devices suited for future energy scenarios. Indeed, SOFCs provide a high electrical efficiency of about 60% with minimum greenhouse gas emissions from a range of possible fuels [1]. To ensure longer operating times of more than 60,000 hours as required target for the commercialization of this technology, there is a need to understand the fundamental degradation mechanisms [2]. It is known that SOFC performance strongly depends on the cell microstructure and its changes under different operation conditions. Past studies have identified several degradation mechanisms associated with the long-term stability of SOFCs under a wide range of operating conditions in terms of temperature, gas composition, fuel utilization etc [3]. These studies have indicated that the most significant changes occur at the fuel electrode in case of the conventional Ni based SOFCs. Indeed, Ni shows a high mobility between 650-950 ˚C, resulting in (i) Ni particle coarsening or agglomeration [4-6], (ii) Ni migration from the active reaction zone close to electrode-electrolyte interface [7-9].

For instance, in Ni-YSZ based fuel electrodes Simwonis et al. [4] showed a decrease of electrical conductivity of 33% over 4000 h operated under 4%mol H_2 and 3%mol H_2O in Argon at 1000 ˚C. This loss was correlated to the reduced number of Ni active particles due to its migration accompanied with agglomeration; here the decrease of Triple Phase Boundary (TPB) length resulted in a worse electrochemical performance as well. Indeed, when the volume fraction of the ionic or electronic phases is below the percolation threshold of 20-35%, a drastic reduction in the TPB length is expected [10]. Hagen et al. [11] also observed changes in the Ni particle diameter and a broader distribution of particle sizes under current densities above 0.75 Acm^{-2} at both 750 ˚C and 850 ˚C. In addition, local Ni depletion was noted at higher operating temperatures in humid conditions, which was attributed to the formation of volatile Ni hydroxide species. Several studies have shown the effect of overpotential on the Ni migration on Ni-YSZ cells. For instance, Hauch et al. [12] detected a significant Ni migration when the fuel electrode overpotentials were between 160 mV and 300 mV. Whereas Sun et al. [13] presented the post-mortem results on 4400 h electrolysis operated cells. In this case, both loss of Ni percolation and increased porosity were observed within the active electrode as consequences of imposed load. Another possible driving force for detected Ni mobility and agglomeration consists of the minimization of surface energy in view of the particle contact areas [14,15]. To validate this hypothesis, Faes et al. [15] studied the grain growth trend for both fine and coarse initial particle size distributions in the Ni cermet electrode. Fine Ni particle sizes resulted in a higher coarsening in the initial 240 h operation as compared to the coarse microstructure of the pristine fuel electrode; the maximum grain size was reached at close to 1000 h. This time profile was simulated using a ‘charging capacitor’ model that assumed the maximum Ni particle growth to be dependent on stable YSZ backbone influence. Monaco et al. [7] recently performed long-term operation tests on Ni-YSZ based cells aged in both fuel cell and electrolysis mode. The Ni particle growth within

* Corresponding author: fiammettarita.bianchi@edu.unige.it

the bulk of the electrode was attributed to local sintering processes due to Ni-YSZ interfacial adhesion gradient, whereas the local overpotential was proposed as the driving force for the Ni detachment and migration at the electrode/electrolyte interface.
Despite the desired target of more than 60,000 h, only few tests exceeding several 1000 hours have been performed in previous scientific literature. For instance, a recent work by Menzler et al. [16] tested a SOFC short stack for 100,000 h at 700 °C, 0.5 Acm^{-2} with humidified H_2 obtaining an overall degradation of 0.5 V% kh^{-1}. Looking at post-mortem analysis, Ni presence increased from 32% to 40% close to the electrolyte/electrode interface with a reduction in the porosity, differently from common reference observations. These uncertainties confirm the need of further studies to obtain a deeper knowledge of occurring mechanisms.
Similar Ni evolution effects were observed also in case of Ni-GDC based fuel electrodes. Holzer et al. [17] studied quantitatively the changes in Ni-GDC cermet under dry and humid conditions (until 40%mol of H_2O). In the first case a rapid reduction of the TPB length was noted due to Ni coarsening in the initial 200 h through Ostwald ripening mechanism [8,18]. At higher operating hours, from 1023 h to 2286 h, Ni volatilization was identified as the main cause for Ni cermet changes resulting in an increase of local Ni-GDC ratio. Whereas, in the humid case GDC formed a layer around the Ni particles which hindered the particle growth. Iwanschitz et al. [19] studied Ni coarsening effects as a function of reduction temperatures for Ni/GDC40 electrode composition, confirming the significant effect of high sintering temperatures on the Ni particle size. Aiming at the validation of cell long-term behaviour Zekri et al. [20] tested Ni-GDC based ESCs with operation times by 20,000 h observing Ni depletion up to 6-10 µm from the electrolyte. Further particle agglomeration effects were observed for both Ni as well as GDC particles throughout the electrode in turn, leading to a higher Ni agglomeration and increased porosity.
Only few studies have shown a direct comparison between the two considered Ni based cermets. For instance, Sciazko et al. [21] analysed Ni-YSZ and Ni-GDC electrode behaviour under both fuel cell and electrolysis operations. Although a better initial performance was observed for the GDC electrodes, Ni-YSZ was concluded to be more durable. Indeed, the YSZ stable backbone limited Ni coarsening effects [15,22]. Whereas the variation of GDC particles resulted in a thicker layer formation outside the reaction zone, which led to a thin more tortuous GDC layer close to the interface.

In this work, the authors aim at studying and comparing 1000 h operated solid oxide fuel cells based on both Ni-YSZ and Ni-GDC fuel electrodes at a fixed fuel feed of 96/4 mol/mol composition of H_2/H_2O and air as the oxidant. An in-situ evaluation of electrochemical performance through voltage measurements and EIS spectra was carried out. A detailed post-mortem analysis of fuel electrode side was also performed showing the main structural changes. These experimental outcomes formed the basis for the tuning of parameters requested into simulation tool. Indeed, a previously validated 2D model, SIMulation of Fuel Cells-SIMFC, was here improved by specifying some kinetic parameters as function of microstructural features to understand the direct correlation between the microstructure variation and the loss of electrochemical performance.

2. Experimental setup

The experimental data were recorded at Technical University of Denmark (DTU) on 4 cm x 4 cm planar commercial cells involving a Ni-YSZ based anode supported cell and a Ni-GDC based electrolyte supported cell. The detailed description of the test setup as well as the characterisation prior and post durability, by varying temperatures, reactant compositions and utilizations, are described elsewhere [23]. The cells were tested under H_2/H_2O molar ratio of 96/4 with air as the oxidant for 1000 hours, as per manufacturer protocols (Table 1). During the durability operation, the cells were characterised using Electrochemical Impedance Spectroscopy (EIS) at intervals of about 8 hours. In case of the ESCs, a N_2 flow was added in order to have the minimum total flows within the test setup. With the added N_2 flow, the effective p_{H2O} in ESC was reduced slightly to ~0.03 atm.

Table 1: Summary of test conditions for the long-term operation of both ASC and ESC configurations.

Parameters	**ASC**	**ESC**
H_2 flow [lh^{-1}]	19.2	9.6
H_2O flow [lh^{-1}]	0.8	0.4
Air flow [lh^{-1}]	140	140
H_2/H_2O ratio [mol/mol]	96/4	96/4
N_2 flow [lh^{-1}]	0	4.6
Total fuel flow rate [lh^{-1}]	20	14.6
Temperature [˚C]	750	850
Current density [Acm^{-2}]	0.4	0.2
Fuel utilization [-]	~14%	~14%

Performance characterization both prior to, after and during durability test was derived by applying a suitable Equivalent Circuit Model (ECM) and Complex Nonlinear Least Squares (CNLS) fitting on recorded EIS spectra. The quantification of different resistances allowed for identification of kinetic parameter dependences on operation conditions. The proposed ECM consists of an inductance element in series with a single ohmic resistor for electrolyte performance and four sub-circuits built up with resistors and constant phase elements in parallel and a Gerischer element in series for behaviour of the electrode [24]. Post-mortem cell analysis was performed by Scanning Electron Microscopy (SEM) and Energy Dispersive X-Ray Analysis (EDS) techniques on a Zeiss Ultra. Secondary electron imaging (SE) was used at high accelerating voltages to study the surface feature changes,

while the percolation network was studied using low accelerating voltages < 1 keV through an in-lens detector. Computed particle sizes and volume fractions were also useful for modelling purposes.

3. Modelling

SOFC performance was simulated based on a 2D approach through SIMFC (SIMulation of Fuel Cells), an in-house developed Fortran code. Dividing the cell plane in an optimised number of sub-cells, the global behaviour derives from a local analysis of conservation equations resolved in each specific subdomain [25]. Here the cell voltage is evaluated through ad hoc formulated electrochemical kinetics and knowing the gradients of main physicochemical features, such as current density, gas composition and temperature, as well as microstructure parameters. Considering an isopotential system, the model assumes Fickian diffusion as the gas transport mechanism inside electrodes, a reaction rate following Butler-Volmer equation and a thermal activated process for the charge transfer. Here SOFC voltage V_{SOFC} results as summarised in Equation 1, then specifying Open Circuit Voltage (OCV), diffusion, activation and ohmic overpotential, η, formulations valid for both anodic and cathodic side in Equations 2, 3, 4 and 5, respectively [26].

$$V_{SOFC} = OCV - \eta_{diff} - \eta_{act} - \eta_{ohm} \quad (1)$$

$$OCV = (RT/zF) \ln [p_{H2,bulk} (p_{O2,bulk})^{0.5} / p_{H2O}] \quad (2)$$

$$\eta_{diff} = (RT/zF) \ln[\Pi (p_{i,bulk}/p_{i,TPB})^{2\alpha i}] \quad (3)$$

$$\eta_{act} = (2RT/zF) \sinh^{-1}(J/J_0) \quad (4)$$

$$\eta_{ohm} = R_{ohm} J = AT \exp(B/T)\, J \quad (5)$$

Where R is the ideal gas constant, T the temperature, z the charge number, p the gas partial pressure, J the current density, J_0 the exchange current density, R_{ohm} the ohmic resistance, A, B and α some kinetic parameters.
Starting from the previously validated approach at time equal to zero for a wide range of working points [23], the model was tuned to simulate the cell behaviour under long-term operation considering the main degradation mechanisms that could penalise the obtainable power. For this purpose, the kinetic parameters obtained from EIS deconvolutions before and after testing were implemented in SIMFC electrochemical kinetics core. Moreover, some empirical coefficients were now formulated as a function of microstructure parameters in order to consider how material changes influence the electrocatalyst active site distribution as well as the conductivity. Here the exchange current density results in function of available active site, namely TPB length l_{TPB}, (Equation 6) or the ohmic term depends on the conductivity σ of each layer (Equation 7).

$$J_0 = 2\gamma l_{TPB} \Pi y_{i,bulk}^{\alpha i} \exp(-E_{act}/RT) \quad (6)$$

$$R_{ohm} = \Sigma (d_j/\sigma_j) \quad (7)$$

Where γ is the preexponential coefficient, E_{act} the activation energy, d the thickness of a specific layer and y the gas molar fraction.
The analysis focused mainly on fuel electrode side which showed a higher variation of performance and microstructure according to experimental observations. Here, for instance the TPB length as well as the cermet conductivity were expressed in terms of particle radius and phase fractions [27].

4. Results and Discussions

The fuel cell performance for both cells was evaluated through electrochemical characterization based on voltage measurements and EIS spectra along with additional information obtained by the SIMFC code, such as the distinction of different polarization losses and their contribution on global cell performance.
Looking at initial operation before durability tests, the Ni-YSZ based anode supported cell shows lower polarization losses as compared to the electrolyte supported cell. For instance, at 800 °C and a current density 0.2 Acm^{-2} the voltage is equal to around 1 V for Ni-YSZ based cell compared to 0.94 V of Ni-GDC based one. According to modelling, indeed the ohmic term increases by a factor of four when moving from the anode supported (Ni-YSZ) to the electrolyte supported (Ni-GDC) design (Figure 1). In addition to the electrolyte thickness effect, also the use of different ceramic materials at the fuel electrode affects the ohmic resistance, since YSZ has a higher conductivity value than GDC (4.2 vs. 2.5 S m^{-1}) [27,28]. Whereas the activation overpotentials are quite similar as well as the diffusion terms that are negligible in both cases.

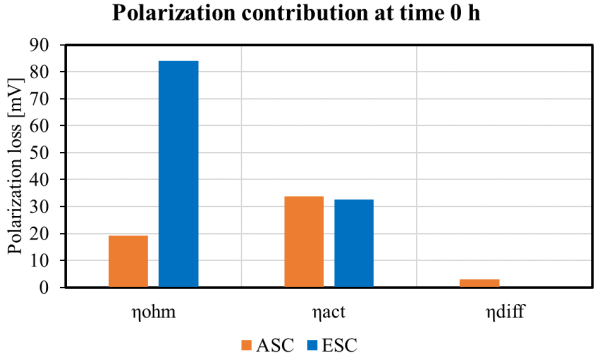

Figure 1. Comparison of polarization losses (ohmic overpotential "ηohm", activation overpotential "ηact" and diffusion overpotential "ηdiff") at 800 °C and 0.2 Acm^{-2} feeding 96/4 H_2/H_2O and air according to SIMFC results.

Durability tests were performed in fuel cell mode avoiding any stressful working conditions such as excessive loads (i.e., cause of fuel starvation), redox and thermal cycles (i.e., cause of delamination and microcracking formation). Here, all detected changes should be specifically correlated to variations in the chosen materials and cell configurations. Figure 2 shows the measured voltage profiles along more than 1000 h operation. In both cases, a gradual reduction is visible

(higher voltage values for Ni-GDC based cell are due to the selected operating conditions specified in Table 1).

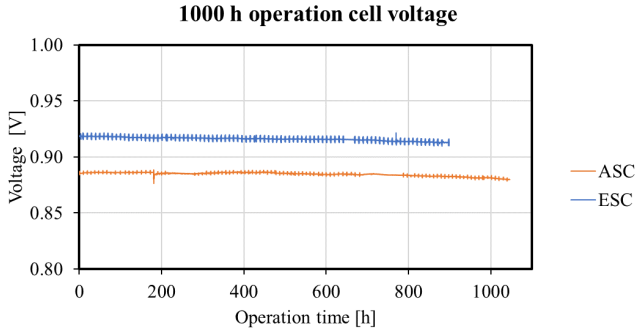

Figure 2. Voltage profiles for cells operated along 1000 h with 96/4 H_2/H_2O fuel composition and air as oxidant at 750 °C under 0.4 Acm^{-2} for ASC (orange line) and at 850 °C under 0.2 Acm^{-2} for ESC (blue line).

A common index of performance variation is the degradation rate *DR* which evaluates the absolute difference between the measured value $V_{SOFC,t}$ at time *t* and the initial voltage $V_{SOFC,0}$, normalised to $V_{SOFC,0}$ assuming a reference time step of 1000 h (Equation 8).

$$DR = \left|(V_{SOFC,t} - V_{SOFC,0})/V_{SOFC,0} \cdot (1000/t)\right| \quad (8)$$

Considering global *DR*, the Ni-YSZ based cell shows a slightly lower value than the Ni-GDC based cell: 0.5 V% kh^{-1} vs. 0.7 V% kh^{-1}. Moreover, the degradation mechanisms are characterised by different trends. The Ni-YSZ based configuration has a larger *DR* in the first 100 operation hours, followed by a fairly stable operation until a further increase of the voltage degradation rate after 350 h. In the last part, *DR* is quite negligible. In comparison, the Ni-GDC based cell shows a continuously decreasing trend until a quite stable *DR* value, suggesting the occurrence of a main degradation processes in the initial test period where *DR* exceeds 10 V% kh^{-1}. Only after 500 h the *DR* becomes always lower than 1 V% kh^{-1} (value reached after only 100 h in ASC case).

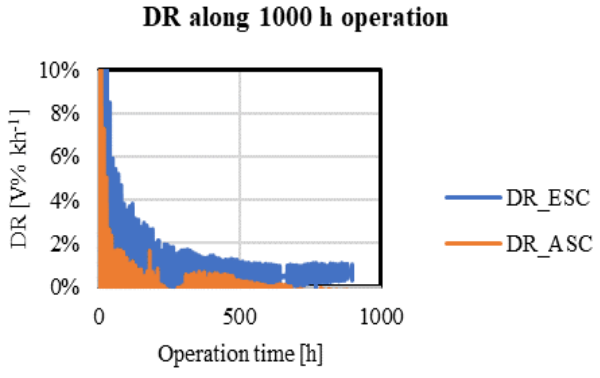

Figure 3. Comparison of degradation rate trends along durability tests.

Figure 4 shows the evolution of the ohmic and polarisation resistances for both configurations. In case of ASC (Figure 4.a), the initial polarisation term is higher than ohmic one of ~0.06 Ωcm^2. This was expected because of the major electrode contribution in terms of activation overpotential (Figure 1). The change of the ohmic resistance decreases from ~145 $m\Omega cm^2kh^{-1}$ in the initial 100 hours to ~4.5 $m\Omega cm^2kh^{-1}$ at 1000 h. Whereas the polarisation resistance shows a linear increasing slope of ~20 $m\Omega cm^2kh^{-1}$ throughout the whole operation. This suggests the main role of electrode degradation to the overall voltage decrease.

In the ESC cell (Figure 4.b), the ohmic contribution is about 1.7 times higher than the polarisation one due to a thicker electrolyte support. Looking at the durability test, the ohmic resistance changes only slightly throughout the whole operation with ~7 $m\Omega cm^2kh^{-1}$ as the maximum value (however it was a smaller degradation rate than ASC cell case). Similar to Ni-YSZ based cell, the polarization resistance has a linear trend with a lower slop equal to ~12 $m\Omega cm^2kh^{-1}$. Despite smaller detected degradation rates for Ni-GDC based cell, more detrimental effects are evident on a global SOFC behaviour due to its higher resistance values.

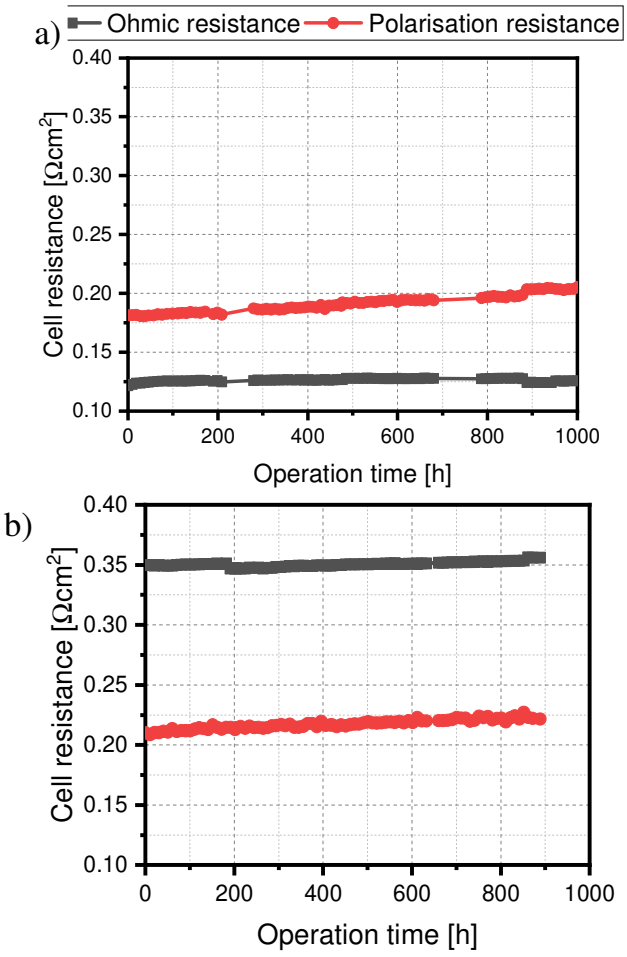

Figure 4. Evolution of ohmic and polarisation resistances over 1000 h operation for a) ASC and b) ESC.

After these preliminary analysis on electrochemical performance of the cells, a detailed post-mortem analysis allowed for the identification of main degradation processes focusing on the fuel electrode structure as discussed earlier. Here SEM image analysis was fundamental to elaborate a more detailed simulation tool where kinetics parameters were expressed as a function also of microstructural features. Since their variations on

the cell plane are not homogeneous, showing different particle sizes and component phases by comparing inlet and outlet sections, the SIMFC local modelling proved to be a suitable tool to represent the cell effective behaviour in long-term operation. Here, maps of main physical, chemical and geometrical features were implemented as inputs for electrochemical kinetics, allowing a correlation between observed microstructural changes and polarization losses.

As an example of this approach, Ni agglomeration and migration detected in the active zone by experimental observations were correlated to TPB length to adjust the anodic overpotential term in ASC case (Equations 4 and 6).

Through post-test SEM analysis, the mean particle diameters and the mean linear intercepts over 1000 particles were determined (Table 2). The global Ni phase fraction is almost unchanged although a more relevant variation in terms of percolating Ni was observed in the samples. Considering particle diameters, Ni underwent coarsening resulting in an overall size increase (a bit higher in the outlet section). Differently the dimension of pores rises in quite homogeneous way showing the same value on the whole cell plane.

Table 2. Microstructure parameters in term of phase fraction and particle size for Ni and pores in ASC.

	Reference	**Inlet after 1000 h**	**Outlet after 1000 h**
	Phase fraction [-]		
Total Ni	40%	39%	37%
Pore	15%	21%	16%
	Mean linear intercept [µm]		
Ni	0.80	1.09	1.15
Pore	0.30	0.49	0.50

These local variations were implemented into the model to evaluate how TPB length changes and to compare the effective anodic overpotential before and after the durability test. At time equal to zero the microstructure is homogeneous in the whole electrode, so a constant value of l_{TPB} was computed equal to 7 µm^{-2}. Whereas for post-test simulation, maps were imposed for Ni radius and fraction distribution as Figure 5.a and Figure 5.b show respectively. According to SIMFC outcomes (Figure 5.c), the availability of TPB active sites decreases as result of the degradation: a Ni radius increase of 35% as well as a Ni percolating phase decrease of 70% cause the l_{TPB} reduction of about 7 times. Looking at specific local values after 1000 h operation, a small increase is observed along the cell feed side due to a higher percolating Ni fraction (27% inlet vs. 30% outlet), indicating a higher impact compared to the increase in particle diameter.

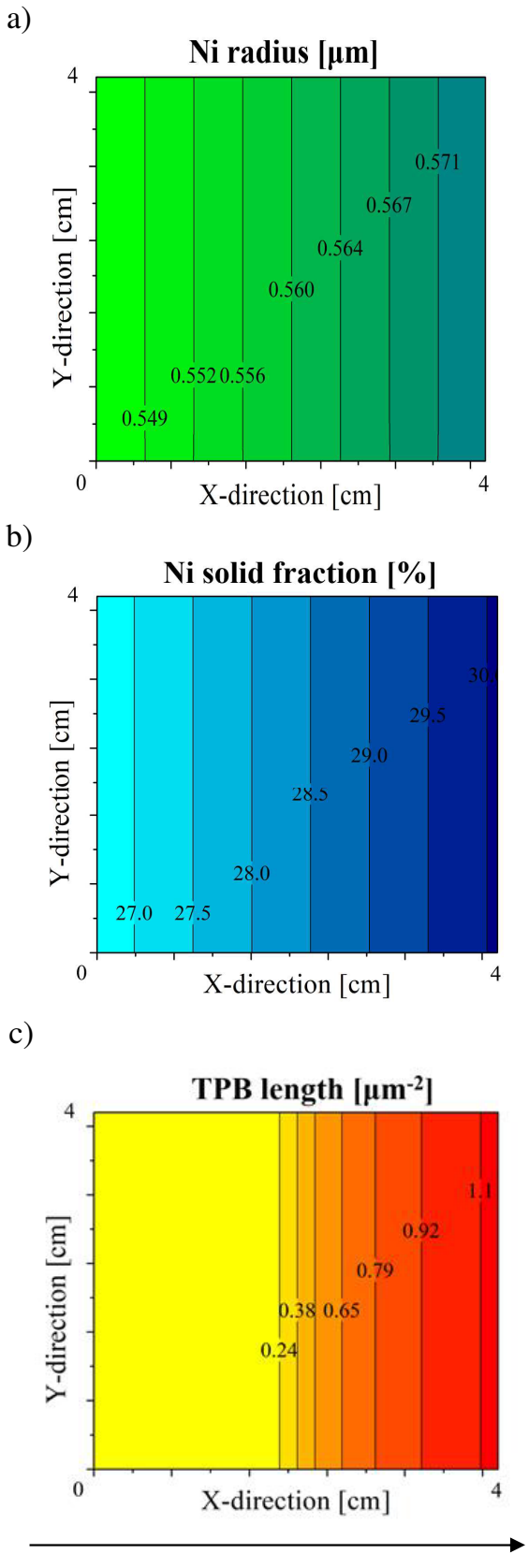

Figure 5. Local maps of imposed a) Ni radius and b) percolating Ni fraction derived from SEM images and c) resulting TPB length computed through SIMFC.

Translating this variation in terms of cell performance and not changing any other kinetic parameter, the

activation overpotential at fuel electrode has a considerable increase by comparing values at time 0 and 1000 operation hours. Considering the case at 750 °C in 96/4 H_2/H_2O fuel composition and dry air as oxidant, Figure 6 shows the increase of η_{act} at fuel electrode under common working points. Here the previously detected increase of TPB length equal to 7 times (at OCV) causes a higher value of activation term around 10 times.
Similar approaches based on experimental observations on microstructural variation and local level modelling could be applied also to determine how material conductivity as well as gas transport phenomena changes influence other polarization losses.

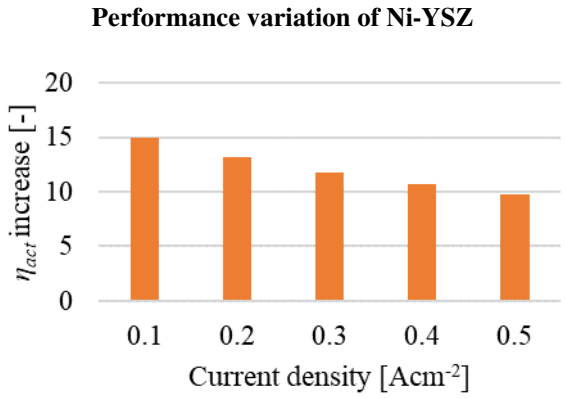

Figure 6. Variation of Ni-YSZ activation overpotential in view of TPB length decrease after 1000 in operation hours.

The results of this research were obtained thanks to received funding from the European Horizon 2020 – Research and Innovation Framework program (H2020-JTI-FCH-2018-1) under grant agreement n°825027 (AD ASTRA project).

References

[1] Elmer, T., M. Worall, S. Wu, S.B. Riffat, Appl. Therm. Eng., 2015, 90, 1082.
[2] Office of energy efficiency & renewable energy. Available online: https://www.energy.gov/eere/fuelcells/downloads/hydrogen-and-fuel-cell-technologies-office-multi-year-research-development. (Accessed on 2020 -11 -24).
[3] Mogensen, M.B., M. Chen, H.L. Frandsen, C. Graves, A. Hauch, P. Vang Hendriksen, T. Jacobsen, S.H. Jensen, T.L. Skafte, X. Sun. Fuel Cells. 2021, 1–15.
[4] Simwonis, D., F. Tietz, D. Stöver, Solid State Ion., 2000, 132(3–4), 241.
[5] Sehested, J., Catal. Today, 2006, 111(1–2), 103.
[6] Yokokawa, H., H. Tu, B. Iwanschitz, A. Mai, J. Power Sources, 2008, 182(2), 400.
[7] Monaco, F., M. Hubert, J. Vulliet, J.P. Ouweltjes, D. Montinaro, P. Cloetens, P. Piccardo, F. Lefebvre-Joud, J. Laurencin, J. Electrochem. Soc., 2019, 166(15), 1229.
[8] Gubner, A., H. Landes, J. Metzger, H. Seeg, R. Stübner, ECS Proc. Vol., 1997, 1997–40(1), 844.
[9] Hauch, A., S.D. Ebbesen, S.H. Jensen, M. Mogensen, J. Electrochem. Soc., 2008, 155(11), B1184.
[10] Martinez, A.S., J. Brouwer, Electrochim. Acta, 2008, 53(10), 3597.
[11] Hagen, A., R. Barfod, P.V. Hendriksen, Y.-L. Liu, S. Ramousse, J. Electrochem. Soc., 2006, 153, A1165.
[12] Hauch, A., K. Brodersen, M.Chen, M.B. Mogensen, Solid State Ion., 2016, 293, 27–36.
[13] Sun, X., P.V. Hendriksen, M.B. Mogensen, M. Chen, FUEL CELLS 19, 2019, 6, 740–747.
[14] Holzer, L., B. Iwanschitz, T. Hocker, B. Münch, M. Prestat, D. Wiedenmann, U. Vogt, P. Holtappels, J. Sfeir, A. Mai, T. Graule, J. Power Sources, 2011, 196(3), 1279.
[15] Faes, A., A. Hessler-Wyser, D. Presvytes, C.G. Vayenas, J. Van herle, Fuel Cells, 2009, 9(6), 841.
[16] Menzler, N.H., D. Sebold, Y.J. Sohn, S. Zischke, J. Power Sources, 2020, 478, 228770.
[17] Holzer, L., B. Münch, B. Iwanschitz, M. Cantoni, T. Hocker, T. Graule, J. Power Sources, 2011, 196(17), 7076–7089.
[18] Ioselevich, A., A.A. Kornyshev, W. Lehnert, J. Electrochem. Soc., 1997, 144(9), 3010.
[19] Iwanschitz, B., L. Holzer, A. Mai, M. Schütze, Solid State Ion., 2012, 211, 69.
[20] Zekri, A., K. Herbrig, M. Knipper, J. Parisi, T. Plaggenborg, Fuel Cells, 2017, 17(3), 359.
[21] Sciazko, A., T. Shimura, Y. Komatsu, N. Shikazono, Bull. JSME J. Therm. Sci. Technol., 2021, 16(1), 2021.
[22] Hubert, M., J. Laurencin, P. Cloetens, B. Morel, D. Montinaro, F. Lefebvre-Joud, J. Power Sources, 2018, 397, 240.
[23] Padinjarethil, A.K.; F.R. Bianchi, B., Bosio, A. Hagen, Conference: European Fuel Cell Forum, 2020.
[24] Graves, C., J. Hjelm, Conference: European Fuel Cell Forum, 2014.
[25] Conti, B., B. Bosio, S.J. McPhail, F. Santoni, D. Pumiglia, E. Arato, Catalysts, 2019, 9(1), 36.
[26] Bianchi, F.R., A. Baldinelli, L. Barelli, G. Cinti, E. Audasso, B. Bosio, Energies, 2020, 13(19), 5058.
[27] Chen, D., W. Bi, W. Kong, Z. Lin, J. Power Sources, 2010, 195(19), 6598–6610.
[28] Leah, R.T., N.P. Brandon, P. Aguir, J. Power Sources, 2005, 145, 336–352.